Dalton Transactions

Ion-conductive metal–organic frameworks

Journal:	*Dalton Transactions*
Manuscript ID	DT-PER-12-2020-004384.R1
Article Type:	Perspective
Date Submitted by the Author:	15-Feb-2021
Complete List of Authors:	Sadakiyo, Masaaki; Tokyo University of Science, Department of Applied Chemistry, Faculty of Science Division I Kitagawa, Hiroshi; Kyoto University, Department of Chemistry

PERSPECTIVE

Ion-conductive metal–organic frameworks

Masaaki Sadakiyo*[a] and Hiroshi Kitagawa*[b]

Received 00th January 20xx,
Accepted 00th January 20xx

DOI: 10.1039/x0xx00000x

Metal–organic frameworks (MOFs) have emerged as a new class of ion conductors because of their tuneable and highly ordered microporous structures. Ionic conduction of various ionic carriers, such as a proton (H^+), hydroxide ion (OH^-), lithium ion (Li^+), sodium ion (Na^+), and magnesium ion (Mg^{2+}), in the pores of MOFs has been widely investigated over the past decade. Reports reveal that the porous or channel structures of MOFs are fundamentally suitable as ion-conducting pathways. There are clear differences in the basic designs of ion-conductive MOFs, i.e., introduction of ionic carriers and construction of efficient ion-conducting pathways, depending on the ionic carriers. We summarize examples and fundamental designs of highly ion-conductive MOFs with verious types of ionic carriers.

1. Introduction

Ionic conduction in solids is one of the important research topics in materials chemistry because of its useful application in energy-related devices, such as secondary batteries[1] and fuel cells.[2] A better understanding of solid-state electrolytes for these cells will contribute to achieving better safety and high-density energy conversion and energy storage systems.[3] Over the past few decades, many researchers have investigated the clear relationship between structure and ionic conductivity using various solids such as metal oxides,[4] metal halides,[5] metal nitrides[6] and others. The ionic conductivity in solids is derived from the migration of ions, which are normally located on lattice points as one of the stable positions. Therefore, the empty spaces (or lattice defect) in the solid for accepting the migrated ions are necessary for the ionic conduction.[7] The structural features of good ionic conductors can be roughly classified into three types. The first is the layered structure or channel (porous) structure that allows the ions to migrate freely in the void spaces (e.g. Na-β-alumina).[8] The second is the mean structure, where the ions can migrate to various lattice points, resulting in averaged occupancy of the ions on these sites (e.g. α-AgI).[9] The third is the defect structure, having some defects on the lattice point and thus the ions located on the neighbouring lattice point can migrate to the next position (e.g. Y-doped ZrO_2).[10]

On another front, metal–organic frameworks (MOFs) have recently attracted much interest as a new class of solids due to their designable pores and wide variety of materials.[11] The porous structure of MOFs is fundamentally suitable for various applications, such as gas storage,[12] separation,[13] catalysis[14] and drug delivery.[15] Over the past decade, many researchers have focused on using the pores of MOFs as spaces or voids for the migration of ions (i.e., ion-conducting pathways), and explored new MOFs that exhibit a high ionic conductivity. Various ions, such as protons (H^+), hydroxide ions (OH^-) and lithium ions (Li^+) have been employed as the ionic carriers in MOFs.

Ionic conductivity (σ(S cm^{-1})) is expressed by the following equation:

$$\sigma = zen\mu$$

where z is the valence of the ionic carrier, e is the elementary charge, n is the carrier concentration and μ is the mobility of the charge carrier. Structural features of MOFs are related to the n and μ. According to this equation, high ionic conductivity can be achieved via both a high concentration of the ionic carrier and high mobility of the ionic carrier. Thus, the creation of ion-conductive MOFs requires addressing the following two features. The first is the introduction of an ionic carrier into the pores of a MOF. The second is the construction of a suitable environment for the mobile ions in the pores (e.g., arrangement of conducting media, ion-conducting pathways). The methodologies to achieve these features will depend on the ionic species. For example, in the case of protons, the introduction of protons directly means the introduction of acids into the MOFs, which is completely different from the introduction of OH^- (a strong base). In addition, the conduction mechanism also depends on the different ions. In particular, a proton exhibits a specific conducting mechanism, the 'Grotthuss mechanism'[16] due to its covalency (described below), which is totally different from other ions such as Li^+. Therefore, an ideal environment for the migration of protons will differ from that required for other ions.

In this review, we summarize ion-conductive MOFs with various ionic carriers, such as protons, hydroxide ions, lithium ions and other ions. We include a historical background,

[a] Department of Applied Chemistry, Faculty of Science Division I, Tokyo University of Science, 1-3 Kagurazaka, Shinjuku-ku, Tokyo 162-8601, Japan.
[b] Division of Chemistry, Graduate School of Science, Kyoto University, Kitashirakawa-Oiwakecho, Sakyo-ku, Kyoto 606-8502, Japan.
† Footnotes relating to the title and/or authors should appear here.
Electronic Supplementary Information (ESI) available: [details of any supplementary information available should be included here]. See DOI: 10.1039/x0xx00000x

fundamental designs and remarkable achievements pertaining to several ion-conductive MOFs.

2. Proton-conductive MOFs

Proton conduction has attracted much interest because of its potential application in fuel cells. In aqueous solution, a proton exhibits abnormally high mobility, 36.2×10^{-8} m^2 s^{-1} V^{-1}, compared with other monovalent cations such as Li^+ (4.0×10^{-8} m^2 s^{-1} V^{-1}) and Na^+ (5.2×10^{-8} m^2 s^{-1} V^{-1}),[17] because of its specific conduction mechanism—the Grotthuss mechanism.[16] The mechanism of proton conduction is traditionally described using two different models: the vehicle mechanism[18] and the Grotthuss mechanism. The vehicle mechanism involves the direct diffusion of protonated ionic species (proton carriers) such as H_3O^+ and NH_4^+, which is similar to other ions. The Grotthuss mechanism is a more efficient model. It allows the protonated species to migrate without the migration of heavy atoms such as an O atom on H_3O^+ through the jump of the protons to neighbouring hydrogen-bonded molecules such as H_2O (Fig. 1). The coexistence of H_2O molecules with protonated H_3O^+ normally results in accelerated proton conductivity, and thus the H_2O molecule is known as the conducting medium in proton conduction.

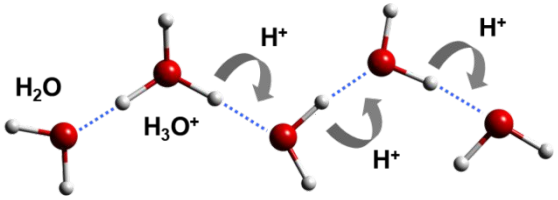

Fig. 1 Schematic illustration of the Grotthuss mechanism in proton transfer.

Various types of proton conductors have been reported, including organic polymers (*e.g.* Nafion®),[19] solid acids (*e.g.* $CsHSO_4$)[20] and metal oxides (*e.g.* Y-doped $BaZrO_3$).[21] However, there is a clear difference in temperature range for high proton conductivity. For example, metal oxides such as Y-doped $BaZrO_3$ require very high temperature (>500 °C) to show high proton conductivity.[21] In contrast, the organic polymer Nafion®, which is used for polymer electrolyte fuel cells, exhibits a very high proton conductivity of $>10^{-2}$ S cm^{-1} at ambient temperature (<80 °C) under humidified conditions.[19] The structure of the proton-conducting pathway inside the Nafion® is a water cluster consisting of adsorbed water molecules (H_2O) and dissociated protons (H_3O^+) provided by the sulfonic acid groups on the polymer chain.[19] This is similar to the situation of proton carriers in aqueous solution, which is one of the ideal systems for efficient proton conduction. However, the amorphous character of the Nafion® does not allow us to visualize the efficient proton-conducting pathway—it should comprise various infinite hydrogen-bonding networks.

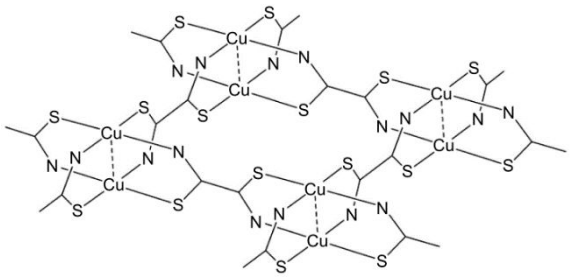

Fig. 2 Fundamental structure of a first reported proton-conductive copper MOF consisting of dithiooxamide-based ligands.

In MOFs, it is protons that are the most widely investigated ionic carriers. Over the past decade, many examples of proton-conductive MOFs have been reported. MOFs have sufficient space for the introduction of both proton carriers (*e.g.* acids, H_3O^+, NH_4^+) and conducting media (*e.g.* H_2O) in their pores, hence potentially suitable for constructing good proton-conducting pathways. In addition, the crystalline character of MOFs offers us an excellent opportunity to visualize the highly proton-conducting pathways (*e.g.* hydrogen-bonding networks) in the pores through X-ray crystallography.

The first proton-conducting MOF was reported by Kanda *et al.* in 1979.[22] They reported a copper MOF (or co-ordination polymer, CP) consisting of a dithiooxamide ligand (Fig. 2). The copper MOF exhibited a proton conductivity of 2.2×10^{-6} S cm^{-1} at 27 °C under humidified conditions (100% relative humidity (RH)). Kitagawa *et al.* also reported ionic conductivity of the derivatives of the copper MOFs having various functional groups. The proton conductivity was ~10^{-6} S cm^{-1}, under similar humidified conditions.[23] These copper MOFs with dithiooxamide ligands had low crystallinity. However, the exact structure inside the pores of these MOFs was not visualized. In 2009, crystalline MOFs showing very high conductivity were reported by three groups. Kitagawa *et al.* reported the fundamental design of proton-conductive MOFs and high proton conductivity of a hydrated MOF that included acidic species.[24] Kitagawa *et al*. and Shimizu *et al*. reported high proton conductivity of crystalline MOFs under non-humid conditions.[25,26] In the decade after 2009, many examples of crystalline MOFs were reported. Hence, the relationship between proton conductivity and the structure of proton-conducting pathways in MOFs has been widely investigated.

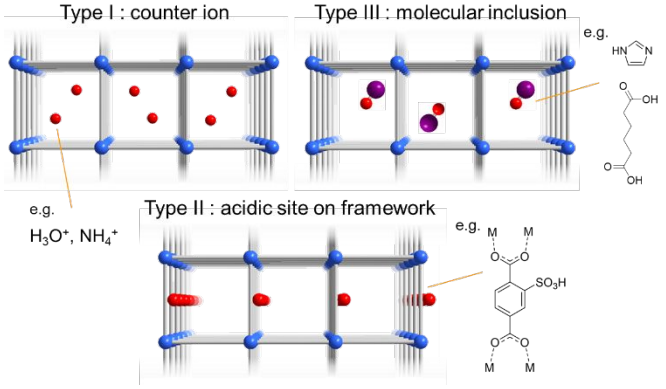

Fig. 3 Schematic illustration of the designs for the introduction of acidic species into MOFs.

High proton conductivity is expected to be achieved through the coexistence of proton carriers (*e.g.* acids, H_3O^+) and conducting media (*e.g.* H_2O). High proton conduction in MOFs requires both the introduction of a proton carrier into the pores and the construction of efficient proton-conducting pathways. Kitagawa *et al.* reported fundamental designs for introducing proton carriers into the pores of MOFs upon consideration of charge compensation (Fig. 3).[24] They classified the designs into three types. Type I uses an anionic framework for introducing the proton carriers into the pores as counter cations. In Type II, acidic groups such as –COOH and $–PO_3H_2$ are introduced on the framework. In Type III, charge-neutral acidic species are incorporated in the voids of the MOFs. Besides these proton carriers, it is preferable that a conducting medium such as H_2O be introduced into the remaining voids in the MOFs for the construction of efficient proton-conducting pathways. Proton carriers can also be generated by self-dissociation. Imidazole and phosphoric acid (H_3PO_4) are known to show high proton conductivity in the liquid state (with no additional protons). This is because the proton carrier is generated by self-dissociation of these molecules (*e.g.* $2H_3PO_4 \leftrightarrow H_4PO_4^+ + H_2PO_4^-$) due to their acid–base property. The self-dissociation of a water molecule, in the liquid phase, is not frequent, as evidenced by the low conductivity of pure water. Therefore, both the introduction of a water molecule with additional proton carriers in the pores and the introduction of imidazole or phosphoric acid molecules in the pores are some of rational ways to achieve high proton conduction in MOFs.

The mechanism of proton conduction is sometimes discussed with the activation energy (E_a) and calculated from the following equation:

$$\sigma T = A \exp(-E_a/kT),$$

where T is temperature, A is a pre-exponential factor and k is the Boltzmann constant. The temperature dependence of conductivity allows us to estimate the value of E_a. The Grotthuss mechanism is considered more efficient than the vehicle mechanism because the long-range proton transport occurs via hydrogen bond cleavage, which requires a very low energy penalty of ~0.11 eV. Therefore, researchers empirically expect that the Grotthuss mechanism gives an activation energy of <0.4 eV.[27]

2-1. Proton conduction in MOFs with H_2O molecules

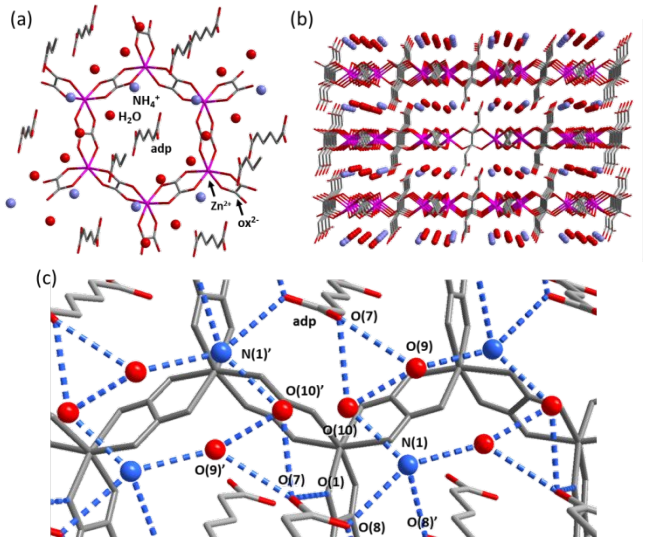

Fig. 4 Representation of the crystal structure of $(NH_4)_2(adp)[Zn_2(ox)_3]\cdot 3H_2O$. (a) Honeycomb-shaped framework. (b) Layered structure along the b axis. (c) Hydrogen-bonding networks located in the interlayer space. Reproduced from ref. 24 with permission from American Chemical Society, copyright 2009.

The water molecule has acid–base properties and can contribute to constructing efficient proton-conducting pathways for the migration of proton carriers. Sadakiyo *et al*. first reported a crystalline MOF that included both acid and water molecules; it exhibited superprotonic conductivity of $\sim 10^{-2}$ S cm^{-1}, which is comparable to an organic polymer (Fig. 4).[24] The composition of the MOF is expressed as $(NH_4)_2(adp)[Zn_2(ox)_3]\cdot 3H_2O$ (adp = adipic acid, ox^{2-} = oxalate), incorporating charge-neutral adipic acid molecules as acidic species in the honeycomb-shaped void. Ammonium ions are also included as acidic species in the interlayer spaces in the anionic framework of $[Zn_2(ox)_3]^{2-}$. Thus, this MOF has both Type I and Type III features. The conducting medium of water molecules is introduced, together with these acids. In the two-dimensional (2D) interlayer space, a 2D hydrogen-bonding network is formed among –COOH, NH_4^+ and H_2O. This MOF exhibited high proton conductivity under high humidity conditions (98% RH): 0.8×10^{-2} S cm^{-1} at 25 °C. Considering the closely located acids and water molecules, the Grotthuss mechanism is expected to dominate. However, this MOF had a relatively high activation energy of 0.63 eV, thought to be derived from a disordered site on an oxygen O(10) atom that shows half occupancy (50%) and with a very short distance between O(10) and O(10)′ (2.189 Å), thus suggesting that a direct jump between these sites should occur for the long-range proton transport.

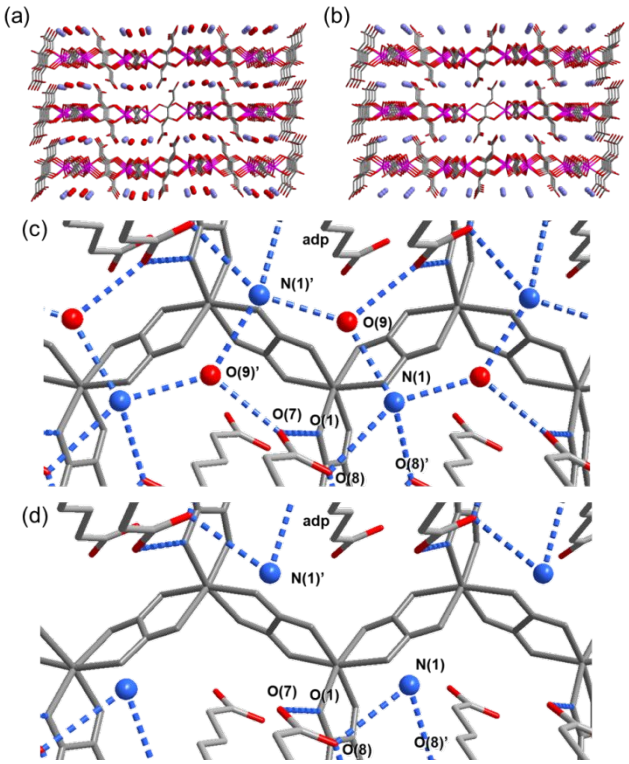

Fig. 5 Representation of the crystal structures: anhydrate and dihydrate phases of $(NH_4)_2(adp)[Zn_2(ox)_3]\cdot nH_2O$. Layered structures of (a) dihydrate and (b) anhydrate phases. Hydrogen-bonding networks of (c) dihydrate and (d) anhydrate phases. Reproduced from ref. 28 with permission from American Chemical Society, copyright 2014.

This compound has two different crystalline phases: dihydrate and anhydrate.[28] Under dehydrated conditions (0% RH), the anhydrate phase is stable. The dihydrate phase is stable in the RH range 10–90%, while the trihydrate phase only exists at very high humidity. The crystal structures of all crystalline phases were determined by single-crystal X-ray diffraction (SCXRD). The dihydrate phase has a similar crystal structure to the trihydrate phase (Fig. 5). There is almost no change in framework structure, except the tilt of adipic acid molecules. However, there is an apparent difference in the hydrogen-bonding network. The number of hydrogen bonds decreases with a decrease in water molecules in the interlayer space. In addition, the length of the hydrogen bonds tends to be greater than in the trihydrate phase. The structure of the anhydrate phase is fundamentally the same as that of the dihydrate phase, *i.e.* no change in the space group, except for the absence of water molecules. Only the anhydrate phase has NH_4^+ ions in the interlayer space; they form local hydrogen bonds with the –COOH groups.

The proton conductivity of the two phases was also evaluated. Measurement of the proton conductivity at various humidities enabled clarification of the relationship between changes in the hydrogen-bonding networks and proton conductivity. The anhydrate phase exhibited a very low conductivity of ~10^{-12} S cm^{-1}, indicating the insulating character of the localized hydrogen-bonding system in the interlayer space. The dihydrate phase exhibited a high proton conductivity of ~10^{-5}–10^{-4} S cm^{-1}, which is much higher than for the anhydrate phase but much lower than for the trihydrate phase (10^{-2} S cm^{-1}). This result clearly demonstrates that this MOF can control the proton conductivity by changing the crystalline hydrogen-bonding networks in the pores and that MOFs offer an excellent platform to determine the exact structure of inner hydrogen-bonding networks, as visualized by X-ray crystallography.

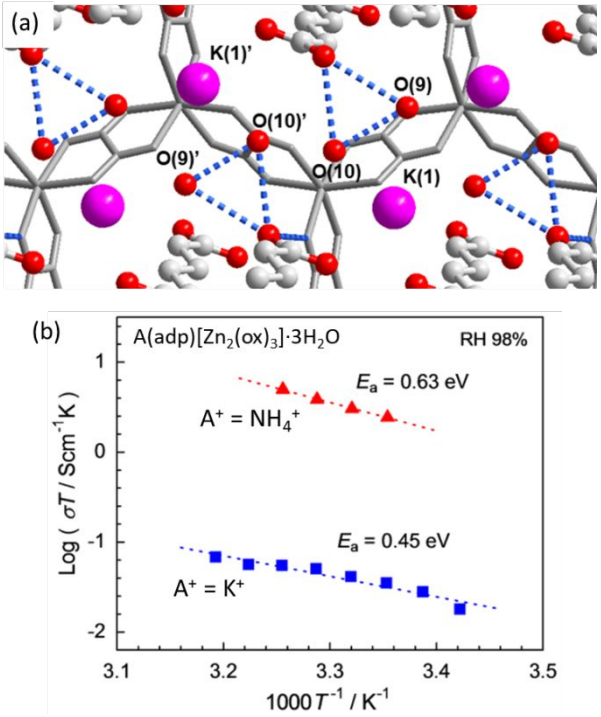

Fig. 6 (a) Representation of the crystal structure of $K_2(adp)[Zn_2(ox)_3]\cdot 3H_2O$. (b) Comparison of ionic conductivity between the ammonium and potassium forms. Reproduced from ref. 29 with permission from American Chemical Society, copyright 2014.

To clarify the role of the NH_4^+ in high proton conductivity, the counter ions of this MOF were substituted by aprotic and non-hydrogen-bonding ions such as K^+ and Rb^+ having similar ionic radii to NH_4^+.[29] These compounds showed almost no change in their crystal structures but did show an apparent change in their hydrogen-bonding networks. Because the K^+ and Rb^+ ions are non-hydrogen-bonding species, the 2D hydrogen-bonding network observed in a NH_4^+ compound disappears in the K^+ and Rb^+ compounds (Fig. 6). There is also an apparent difference in their proton conductivities. Both the K^+ and Rb^+ compounds exhibited a much lower proton conductivity (~100 times lower, ~10^{-4} S cm^{-1}): the K^+ compound 1.2×10^{-4} S cm^{-1} (25 °C, 98% RH) and the Rb^+ compound 4.3×10^{-5} S cm^{-1} (25 °C, 98% RH). This difference in the conductivity is probably derived from a change in the hydrogen-bonding network—the proton carrier would have been derived mainly from the –COOH group due to its higher acidity than NH_4^+. Thus, it is clear that the NH_4^+ assists in the construction of proton-conducting pathways in this MOF. Further studies on the proton dynamics in NH_4^+ and K^+ compounds using neutron scattering revealed that the

existence of NH_4^+ also affects the motion of the neighbouring molecules.[30]

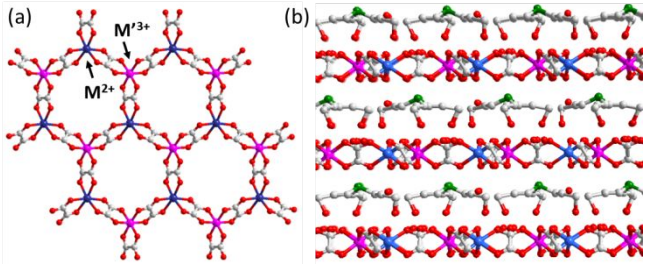

Fig. 7 Representation of the fundamental structures of a mixed valence $[M^{II}M'^{III}(ox)_3]^-$ framework. (a) Honeycomb-shaped 2D framework consisting of M^{2+} and M'^{3+}. (b) Location of the cations in the interlayer space, exemplified by $\{NH(prol)_3\}[MM'(ox)_3]\cdot nH_2O$. Reproduced from ref. 32 with permission from American Chemical Society, copyright 2009.

Ōkawa *et al.* reported a series of similar oxalate-bridged 2D MOFs, showing the coexistence of magnetism and proton conduction—this 2D framework is traditionally reported as a magnetic framework.[31] A mixed valence MOF, $\{NH(prol)_3\}[MCr(ox)_3]\cdot nH_2O$ ($NH(prol)_3^+$ = tri(3-hydroxypropyl)ammonium; M = Mn^{2+}, Fe^{2+}, Co^{2+}) has been reported as a MOF showing the coexistence of ferromagnetism and proton conduction (Fig. 7).[32] The frameworks comprising mixed valent central metals of Cr^{3+} and M^{2+} exhibit ferromagnetic behaviour at low temperature (<10 K). The transition temperature depends on the M^{2+}, *i.e*. Mn^{2+}, Fe^{2+} and Co^{2+}, corresponding here to 5.5, 9.0 and 10.0 K. On the other hand, the proton conductivity of these compounds does not strongly depend on the central metals. The proton conductivity was estimated to be ~10^{-5} S cm^{-1} (25 °C, 83% RH). These authors also measured the conductivity of $\{N(n\text{-}C_4H_9)_4\}[MnCr(ox)_3]$ having the same 2D framework with a non-protic cation. This MOF exhibited an insulating character (10^{-12} S cm^{-1}), indicating that the proton conduction of $\{NH(prol)_3\}[MCr(ox)_3]$ is derived from the protic cations and adsorbed water molecules. Another example, $\{NR_3(CH_2COOH)\}[MCr(ox)_3]\cdot nH_2O$ (R = Me (methyl), Et (ethyl) or Bu (n-butyl) and M^{2+} = Mn^{2+} or Fe^{2+}), was reported; it was a similar MOF in that it exhibited higher proton conductivity because of the higher acidity of the included cation, $NR_3(CH_2COOH)^+$.[33] The hydrophilicity of this MOF is controlled by changing the length of the alkyl chain of the included cation. The cation with a methyl group, $NMe_3(CH_2COOH)^+$, exhibited the greatest hydrophilic character and enabled the MOF $\{NMe_3(CH_2COOH)\}[MCr(ox)_3]\cdot nH_2O$ to exhibit a high proton conductivity of 10^{-4} S cm^{-1} (25 °C), even at low humidity (65% RH). Water vapour adsorption measurements revealed that this high proton conductivity at low humidity is derived from the high adsorption of water molecules even at low humidity. In contrast, $\{NBu_3(CH_2COOH)\}[MCr(ox)_3]\cdot nH_2O$, having the butyl group, has a very hydrophobic character; it exhibits low water adsorption and low proton conductivity (10^{-11} S cm^{-1}) under similar conditions (60% RH). Employing the same 2D framework with mixed valent Fe^{m+}, $\{NEt_3(CH_2COOH)\}[FeFe(ox)_3]\cdot nH_2O$ shows the coexistence of proton conduction and Néel N-type ferrimagnetism.[34]

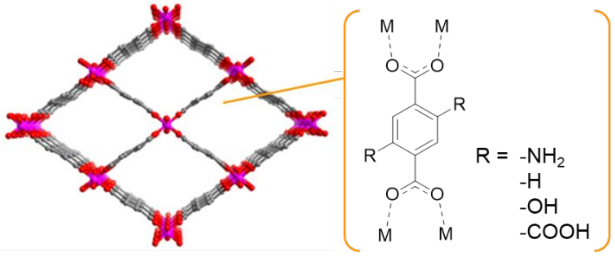

Fig. 8 Schematic illustration of MIL-53-based proton-conductive MOFs having various functional groups on the framework.

Shigematsu *et al.*[35] reported the proton conductivity of a series of MOFs, having various functional groups, on a MIL-53-based framework. They compared the proton conductivity of MIL-53-based MOFs, [M(OH)(bdc–R)] (M^{3+} = Al^{3+} or Fe^{3+}, bdc^{2-} = 1,4-benzenedicarboxylate), including various functional groups of the –R (such as –COOH, –H, $–NH_2$ and –OH) (classified as a Type II compound) (Fig. 8). The one-dimensional (1D) channels of MIL-53 can adsorb water molecules and then show proton conduction by a protonic carrier provided by the functional groups, *i.e*. acidic sites. Their systematic study revealed that proton conductivity in the range 10^{-8}–10^{-5} S cm^{-1} under humidified conditions (25–80 °C, 95% RH) strongly depends on the functional groups. The MOF with carboxylic acid groups exhibited the highest conductivity. The order of proton conductivity of MOFs with other functional groups is –COOH > –OH > –H > $–NH_2$, thus confirming that the acidity of the functional group is a critical factor for proton conduction in this compound because the proton carriers are provided by them. The values of the activation energy were in the range 0.47–0.21 eV, indicating that the Grotthuss-type mechanism constitutes the dominant mechanism in the proton conduction of these MOFs.

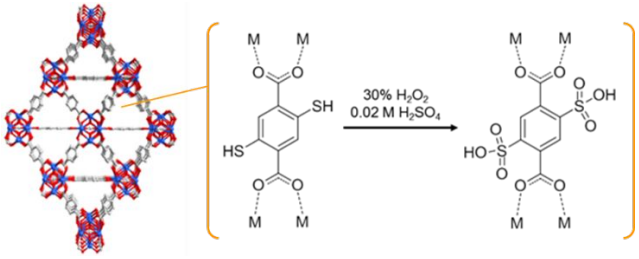

Fig. 9 Schematic illustration of the framework structure and the post-synthetic method used to create a proton-conductive MOF, UiO-66-SO_3H. Reproduced from ref. 36 with permission from Wiley-VCH, copyright 2015.

In a Type II compound, the proton carriers are provided by the dissociation of the acidic sites on the framework. Thus, highly acidic functional groups, such as $–PO_3H_2$ and $–SO_3H$, are preferable for high proton conduction. However, the successful introduction of such highly acidic species into MOFs is not an easy task because MOFs are not very stable upon exposure to strong acidic or basic conditions, because their construction includes Lewis acid (central metal) and base (ligand).

Phang *et al.* reported on the introduction of a very strong acid, a sulfonic acid group (–SO_3H), on the framework of UiO-66 that has strong acid tolerance (Fig. 9).[36] They succeeded in introducing the –SO_3H through a post-synthesis method. UiO-66$(SH)_2$, having a –SH group on the UiO-66 framework, was first synthesized using H_2DMBDC ligand (2,5-dimercapto-1,4-benzenedicarboxylic acid). The –SH group on UiO-66 was then converted into a –SO_3H through an oxidation reaction with H_2O_2 under acidic conditions. The synthesized sample UiO-66(SO_3H) exhibited very high proton conductivity of 8.4×10^{-2} S cm^{-1} under humidified conditions (80 °C, 90% RH). This amazingly high value of proton conductivity of UiO-66(SO_3H) clearly demonstrates that the acidity of the functional group in a Type II compound is important for high proton conduction. The activation energy was estimated to be 0.32 eV. This is indicative that the Grotthuss-type mechanism is included in this compound. It is noteworthy that the sample prior to post-synthesis, UiO-66$(SH)_2$, does not show high conductivity (2.5×10^{-5} S cm^{-1}) because of the weak acidic character of the –SH group.

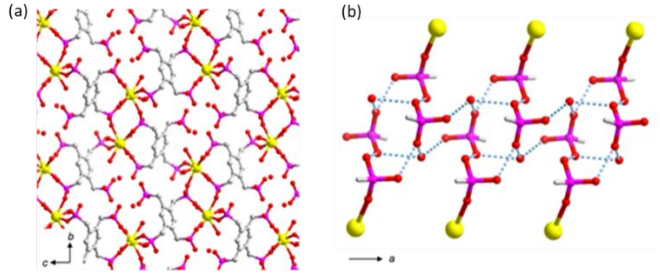

Fig. 10 Representation of the crystal structure of PCMOF-5: (a) framework structure and (b) hydrogen-bonding networks. Reproduced from ref. 37 with permission from American Chemical Society, copyright 2013.

Taylor *et al.* reported a Type II compound with phosphonic acid groups (–PO_3H_2), which also have very strong acidity. The phosphonic acid-included MOF, $[La(H_5L)(H_2O)_4]$ (PCMOF-5, L = 1,2,4,5-tetrakis(phosphonomethyl)benzene), was synthesized using the 1,2,4,5-tetrakis(phosphonomethyl)benzene ligand (Fig. 10).[37] The water molecule was also introduced, as a coordinating water, on the framework. The introduced –PO_3H_2 and water molecules form a complicated hydrogen-bonding network as a proton-conducting pathway. This MOF had a very high proton conductivity of 1.3×10^{-3} S cm^{-1} at ambient temperature (21.5 °C, 98% RH). The activation energy was 0.16 eV, hence suggesting that the Grotthuss-type mechanism is included. This is consistent with findings pertaining to the closely-packed structure of –PO_3H_2 and water molecules, which is expected to work as a conducting medium. It is noteworthy that this activation energy is the lowest value recorded for proton-conducting MOFs, hence suggesting that the hydrogen-bonding network with acid and water is one of the ideal proton-conducting systems, even in solid-state materials.

Grain boundary contribution in proton conduction is one of the discussing topics in proton-conducing MOFs. Wong *et al.* reported a series of the MOFs mentioned above, $[Ln(H_5L)(H_2O)_4]$, using different central metals of lanthanoid (Ln) elements, such as Ce, Pr, Nd, Sm, Eu and Gd.[38] The La and Pr compounds exhibited very high proton conductivity of $>10^{-3}$ S cm^{-1}, while the other compounds exhibited conductivity of $\sim10^{-4}$ S cm^{-1}. They evaluated the morphology and grain size of the microcrystals of these compounds using scanning electron microscope (SEM) and found that the difference in proton conductivity is attributable to the difference in grain size of the resulting crystals. This is indicative that grain boundary contribution in proton conduction is one of the important factors of proton conduction. In addition, they also prepared a ball-milled sample of La-PCMOF-5, that has different morphology and smaller grain size (averaged size is 1.14 μm) compared to pristine La-PCMOF-5 (1.71 μm). The milled sample showed lower conductivity of 1.3×10^{-4} S cm^{-1} that the conductivity of the pristine sample (6.0×10^{-3} S cm^{-1}), indicating that the degradation or dissolution of the MOF at the particle surface does not dominantly contribute to the ionic conductivity in this compound. Tominaka *et al.* also discussed the grain boundary contribution in proton conductivity of a MOF. They reported a large difference in proton conductivity between powder sample of nonporous MOF, Fe(ox)·$2H_2O$, and its single crystal.[39] The powder sample of Fe(ox)·$2H_2O$ showed high proton conductivity around 10^{-3} S cm^{-1} at room temperature. However, the single crystal of Fe(ox)·$2H_2O$ showed low proton conductivity around 10^{-9} S cm^{-1}. This is indicative that grain boundary contribution is dominant compared to the bulk contribution and that efficient proton-conducting pathway formed around the interparticle phases in this MOF. These examples suggested that the grain boundary contribution is often hardly distinguishable from bulk one from a single impedance component. Xu *et al.* reported proton conductivity of a surface MOF showing very high conductivity around 3.9×10^{-3} S cm^{-1} at room temperature.[40] The surface MOF is dominantly composed of the surface (i.e., similar to grain boundary) rather than the bulk. They mentioned that this high conductivity on the surface would be derived from some dangling functional groups. This result is also indicative that the surface (or grain boundary) conduction is often more considerable than the conduction in bulk crystal.

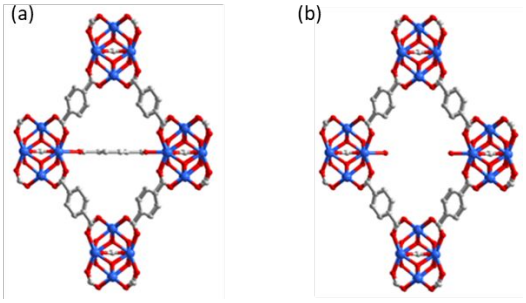

Fig. 11 Schematic representation of crystal structures of (a) UiO-66 and (b) UiO-66 with defects of ligands. Reproduced from ref. 41 with permission from American Chemical Society, copyright 2015.

The introduction of acidic groups such as –PO_3H_2 on the framework is a typical way to introduce proton carriers into the MOFs with the Type II feature. However, Taylor *et al.* reported

a new approach for the introduction of a proton carrier with the Type II feature. This involves defect engineering of the UiO-66 framework (Fig. 11).[41] The authors introduced defect sites on the UiO-66 framework (expected to work as Lewis acidic sites) by changing synthetic parameters such as solvents or modulating ligands (*e.g.* acetic acid). The modulated samples have the same crystal structures but different proton conductivity, in the range 10^{-5}–10^{-3} S cm^{-1} (60 °C, 95% RH), indicating that the defect engineering can control the proton conductivity and that the defect can be a proton source, as an acidic site on the framework. The highest proton conductivity was observed in the sample with 1.0 stearic defects per formula: 6.8×10^{-3} S cm^{-1}. Modulated samples also had various values of activation energy values, in the range 0.22–0.36 eV. The very low activation energy is indicative that these samples include the Grotthuss-type mechanism, due to the existence of water molecules in the pores under the highly humidified condition.

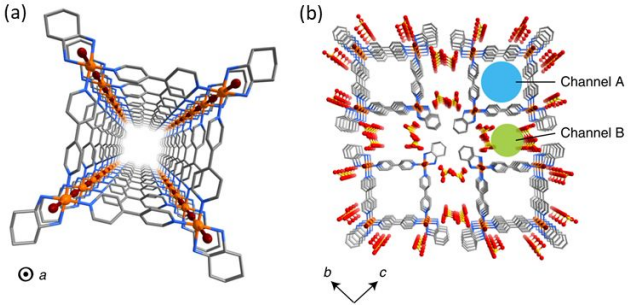

Fig. 12 Representation of the crystal structure of [Pt(dach)(bpy)Br]$_4$(SO$_4$)$_4$·32H$_2$O: (a) tubular structure and (b) locations of the channels, including water molecules.

Otake *et al*. reported another unique example of introducing a protonic carrier using a Lewis acidic site. They reported a tubular MOF, [Pt(dach)(bpy)Br]$_4$(SO$_4$)$_4$·32H$_2$O (dach = (1R, 2R)-(–)-1,2-diaminocyclohexane; bpy = 4,4′-bipyridine), including a large number of water molecules with no acidic species (Fig. 12).[42] This MOF exhibited very high proton conductivity: 1.7×10^{-2} S cm^{-1} (50 °C, 95% RH). SCXRD and ^{1}H NMR studies revealed that the hydrogen-bonding network among the introduced water molecules in the 1D channel inside the tubular framework plays as a critical role in the high proton conduction. DFT calculations revealed that the proton carriers are provided by the amino group on the dach ligand, coordinating to the Pt^{4+} ion, because the coordinating amino group presents as an acid, having similar acidity to a carboxylic acid due to the Lewis acidity of the high valent Pt^{4+} ion. This MOF was also classified as a Type II compound.

2-2. Proton conduction in MOFs under anhydrous condition

Proton conductors in which molecules are used as conducting media require humidified conditions to retain the water molecules inside the materials. Therefore, such water-based proton conductors will show high ionic conductivity above 100 °C because of the desorption of the adsorbed water molecules. For fuel cell applications, non-humidified conditions, with the temperature slightly above 100 °C, is considered ideal, because then humidifiers, cooling systems and large amounts of catalyst are not required. Thus, the development of proton conductors that exhibit high conductivity under such non-humidified conditions, >100 °C, is required.

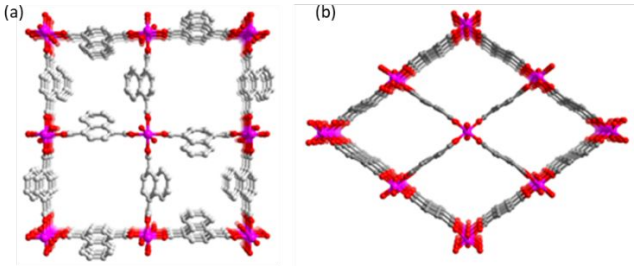

Fig. 13 Representation of framework structures of anhydrous proton conductors: (a) [Al(μ_2–OH)(1,4-ndc)]$_n$ and (b) [Al(μ_2–OH)(1,4-bdc)]$_n$.

Considering the volatility of the water, non-volatile conducting media such as imidazole or phosphoric acid could be suitable molecules to be introduced into the pore of MOFs for achieving high proton conduction under anhydrous conditions. Bureekaew *et al.* reported two MOFs, [Al(μ_2–OH)(1,4-ndc)]$_n$ (1,4-ndc^{2-} = 1,4-naphthalenedicarboxylate) and [Al(μ_2–OH)(1,4-bdc)]$_n$ (1,4-bdc^{2-} = 1,4-benzenedicarboxylate), incorporating imidazole molecules in their pores (Fig. 13).[25] These imidazole-included MOFs were prepared by adsorption of imidazole vapour at 120 °C, after dehydration of the frameworks. [Al(μ_2–OH)(1,4-ndc)]$_n$ has two types of 1D channels with sizes of 7.7×7.7 Å^2 and 3.0×3.0 Å^2, while [Al(μ_2–OH)(1,4-bdc)]$_n$ has a 1D channel with a size of 8.5×8.5 Å^2. Because the small channel of [Al(μ_2–OH)(1,4-ndc)]$_n$ cannot adsorb an imidazole molecule (4.3×3.7 Å^2), the loading amount of imidazole in [Al(μ_2–OH)(1,4-bdc)]$_n$ is greater than that in [Al(μ_2–OH)(1,4-ndc)]$_n$. However, the proton conductivity of [Al(μ_2–OH)(1,4-ndc)]$_n$ with imidazole (2.2×10^{-5} S cm^{-1}, 120 °C) is much higher than that of [Al(μ_2–OH)(1,4-bdc)]$_n$ with imidazole (1.0×10^{-7} S cm^{-1}, 120 °C). Solid-state ^{2}H NMR measurements of these compounds revealed that this difference in proton conductivity is derived from a difference in molecular motion of the included imidazole molecules. The mobility of imidazole molecules in [Al(μ_2–OH)(1,4-ndc)]$_n$ is higher than that in [Al(μ_2–OH)(1,4-bdc)]$_n$ over the entire temperature range. In these compounds, proton conduction should occur through a Grotthuss mechanism, by means of the proton transfer between imidazole molecules. The ionic carrier should be derived from the self-dissociation of imidazole. Therefore, differences in molecular motion of imidazole molecules are directly related to the ionic conductivity.

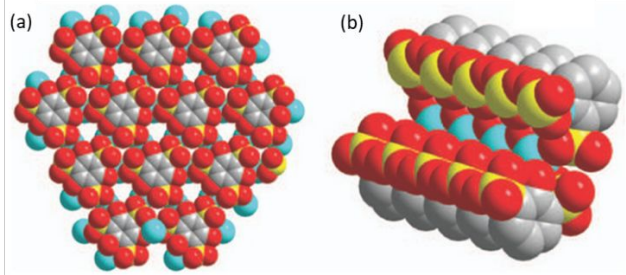

Fig. 14 Representation of the crystal structure of β-PCMOF2: (a) framework and (b) channel structure. Reproduced from ref. 26 with permission from Nature Publishing Group, copyright 2009.

Hurd *et al.* reported a proton-conductive MOF, [Na_3(2,4,6-trihydroxy-1,3,5-benzenetrisulfonate)] (abbreviated to β-PCMOF2), having 1D channels (Fig. 14).[26] This MOF includes water molecules after synthesis. Thus, β-PCMOF2(H_2O)$_{0.5}$ exhibits some proton conductivity: 5.0×10^{-6} S cm^{-1} (30 °C). However, after heating, the conductivity decreased to $<10^{-8}$ S cm^{-1}, due to dehydration. The authors then introduced 1*H*-1,2,4-triazole (Tz) into the empty pores of β-PCMOF2, using various amounts of Tz (yielding β-PCMOF2(Tz)$_{0.3}$, β-PCMOF2(Tz)$_{0.45}$ and β-PCMOF2(Tz)$_{0.6}$). All the Tz-included samples exhibited very high conductivity: $\sim10^{-4}$ S cm^{-1} at >100 °C. The maximum conductivity reached 5×10^{-4} S cm^{-1} at 150 °C. Considering that the β-PCMOF2 does not exhibit high ionic conductivity, these conductivities are derived from the included Tz molecules. The authors also applied β-PCMOF2 in an electrochemical cell: H_2, Pt,C|β-PCMOF2(Tz)$_{0.45}$|Pt,C, air. Using the MOF as an electrolyte, an open circuit voltage (1.18 V at maximum) was observed above 100 °C.

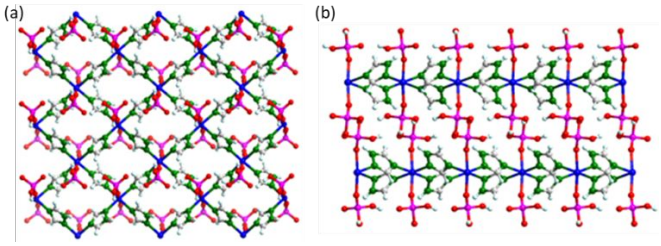

Fig. 15 Representation of the crystal structure of [$Zn(H_2PO_4)_2(TzH)_2]_n$: (a) 2D framework structure and (b) layered structure. Reproduced from ref. 43 with permission from American Chemical Society, copyright 2012.

Umeyama *et al*. reported a proton-conductive MOF, [$Zn(H_2PO_4)_2(TzH)_2]_n$ (TzH = 1,2,4-triazole), having protonated phosphoric acid on the framework (Fig. 15).[43] The anhydrous proton-conductive MOFs mentioned above are constructed by the introduction of conducting media, such as imidazole, into the empty pores of MOFs. However, this compound does not have a significant porous structure, but has anhydrous hydrogen-bonding networks among the H_2PO_4 that is co-ordinated on Zn^{2+} ions. This MOF exhibited a very high proton conductivity of 1.2×10^{-4} S cm^{-1} (150 °C) under anhydrous conditions. The authors also determined the anisotropy of proton conductivity using a single crystal. The proton conductivity along the hydrogen-bonding network was estimated to be 1.1×10^{-4} S cm^{-1} at 130 °C, while that along the perpendicular direction was 2.9×10^{-6} S cm^{-1} at 130 °C, indicating that the proton conduction occurs efficiently through the hydrogen-bonding network of anhydrous H_2PO_4.

3. Hydroxide ion-conductive MOFs

Hydroxide ion conduction has also attracted much attention because of its useful application in alkaline fuel cells, which can then operate without the requirement for costly precious metal catalysts, such as Pt. The hydroxide ion (OH^-) also shows unusually high mobility in aqueous solution (20.6 m^2 s^{-1} V^{-1}), compared to other ions, similar to that in the case of protons. Theoretical calculations have revealed that this abnormal mobility can be explained by a specific motion in hydroxide ion transport together with 'proton back-transfer'.[44] In this motion, hydroxide ions can migrate by accepting protons from neighbouring H_2O molecules through the hydrogen bonds—similar to that in the Grotthuss-type mechanism in proton conduction. Thus, hydroxide ions are also expected to exhibit high ionic conductivity with protic conducting media, such as water molecules. The introduction of hydroxide ions into the pores of MOFs, together with a conducting medium such as water molecules, is therefore a rational way to create hydroxide ion-conductive MOFs.

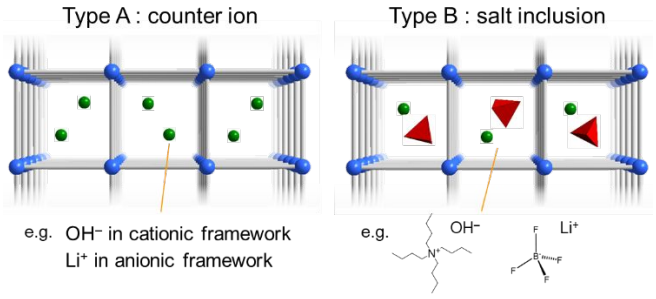

Fig. 16 Schematic illustration of the designs for the introduction of other ionic species into MOFs.

Sadakiyo *et al.* first reported basic designs for the introduction of hydroxide ions into MOFs.[45] The methodology for the introduction of other ions, such as hydroxide ions can be classified into two types (Fig. 16). In Type A, hydroxide ions are introduced directly into cationic frameworks as counter ions. In Type B, hydroxide ions are introduced together with counter cations as hydroxide salts. It is noteworthy that MOFs are usually unstable towards strong base—besides some alkaline-stable MOFs such as ZIF-8.[46] Thus, the mother framework should be carefully selected. The authors synthesized a hydroxide ion-included MOF, $(NBu_4)_m(A)_n\{Zn(mim)_2\}_6$ (Hmim = 2-methylimidazole; A = anions such as OH^-), using ZIF-8 as the mother framework. This MOF incorporates a hydroxide salt of NBu_4OH in the pores, indicating the Type B feature (Fig. 17).[45] The hydroxide ion-included MOF exhibited a proton conductivity of 2.3×10^{-8} S cm^{-1} (25 °C, 99% RH), which is much higher than that of the ZIF-8 itself (10^{-12} S cm^{-1}). Water vapour adsorption measurements revealed that this conductivity is derived from the included hydroxide ions and water molecules, under humidified conditions. Although this compound is expected to show good conduction through proton back-transfer, as described above, because of the coexistence of both hydroxide ions and water molecules, the activation energy of this compound was estimated to be 0.7 eV. This relatively high activation energy is attributed to the small apertures of ZIF-8.

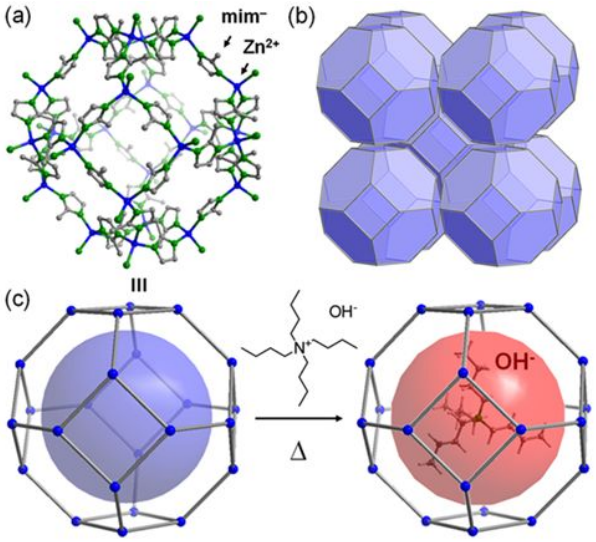

Fig. 17 Representation of the crystal structure of the ZIF-8-based hydroxide ion-conductive MOF: (a) cage, (b) 3D sodalite-type structure of the mother framework and (c) introduction of hydroxide ion salt into the mother framework. Reproduced from ref. 45 with permission from American Chemical Society, copyright 2014.

Li *et al.* reported another example of a Type B compound. They synthesized $[Cu_6(NDI)_3]$·Guests (H_2NDI = 2,7-bis(3,5-dimethyl)dipyrazol-1,4,5,8-naphthalene-tetracarboxydiimide), including various hydroxide salts. $[Cu_6(NDI)_3]$ is a charge-neutral framework and has very high stability towards base.[47] The hydroxide ion is incorporated together with various cations, such as NBu_4 and EVIm (1-ethyl-3-vinylimidazolium). This MOF exhibited very high conductivity: 10^{-7}–10^{-2} S cm^{-1} (30 °C, 95% RH). $[Cu_6(NDI)_3]$·[EVIm]OH exhibited the highest conductivity of 5.7×10^{-2} S cm^{-1}. The activation energy of this compound was estimated to be 0.11 eV, which is indicative that the ionic conduction occurs through a Grotthuss-like mechanism with the proton back-transfer.

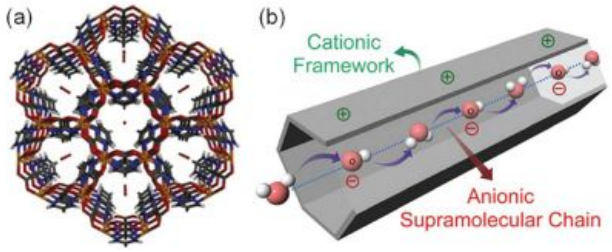

Fig. 18 (a) Representation of the crystal structure of $[Ni_2(m\text{-}pymca)_3]OH{\cdot}nH_2O$. (b) Schematic illustration of hydroxide ion conduction in the 1D channel of the MOF by the introduced water molecules and hydroxide ions. Reproduced from ref. 48 with permission from Royal Society of Chemistry, copyright 2016.

A hydroxide ion-conductive MOF of Type A has also been reported. Nagarkar *et al.* reported a hydroxide ion-conductive MOF, $[Ni_2(m\text{-}pymca)_3]OH{\cdot}nH_2O$, having a cationic framework including hydroxide ions in the pores (Fig. 18).[48] In the 1D channels of this compound, the included hydroxide ions and water molecules form a hydrogen-bonding network, which seems to be one of the ideal systems for efficient migration of hydroxide ions with the proton back-transfer. This compound exhibited a very high ionic conductivity of 0.8×10^{-4} S cm^{-1} (27 °C, 99% RH) under humidified conditions. A large difference in ionic conductivity between the samples under H_2O and D_2O conditions indicates that the proton back-transfer process is included in the ionic conduction. The activation energy was estimated to be 0.19 eV, which is comparable to general proton conductors with a Grotthuss-type mechanism.

4. Conduction of other ionic carriers in MOFs.

As mentioned above, protons and hydroxide ions have an efficient conducting mechanism in some conducting media, such as water and imidazole molecules. Thus, these ions are fundamentally suitable to migrate in MOFs because the MOFs have an ability to incorporate both the ions and the conducting media. For other ions, such as Li^+, Na^+ and Mg^{2+}, MOFs also show great potential to be highly ion-conductive materials due to their ability to incorporate the ionic carriers and additional space as the conducting pathway for these ions. Considering the charge compensation of MOFs, the methodology for the introduction of these ions can also be classified into two types: Type A (counter ions of framework having opposite charge) and Type B (inclusion with counter ions as its salt), as is the case with the hydroxide ion-conductive MOF (Fig. 16).

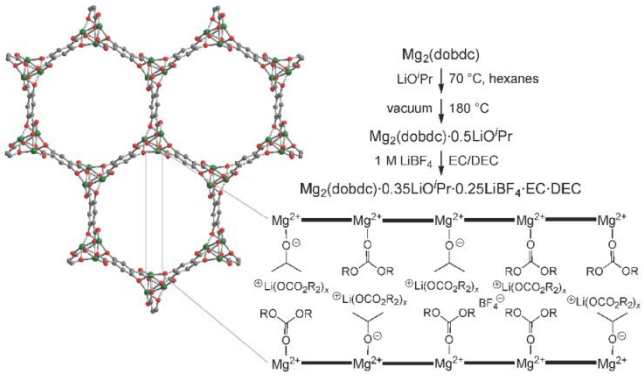

Fig. 19 Schematic representation of the framework structure and synthetic strategy of the lithium ion-conductive MOF, Mg(dobdc) with lithium salts. Reproduced from ref. 49 with permission from American Chemical Society, copyright 2011.

The lithium ion is one of the most important ionic carriers in solid-state ionics because of the potential application in secondary batteries. Wiers *et al.* reported lithium ion conduction in a MOF, Mg(dobdc) (dobdc^{4-} = 1,4-dioxido-2,5-benzenedicarboxylate), having 1D channels with open metal sites as Lewis acidic sites (Fig. 19).[49] The lithium ion salts LiO^{i}Pr and $LiBF_4$, are incorporated into this MOF with guest solvents such as ethylene carbonate and diethyl carbonate, indicating that this compound has the Type B feature. The Lewis acidic site, the open metal site of Mg^{2+} on the framework, is expected to trap the anions through co-ordination. They synthesized Mg(dobdc) with $LiBF_4$, LiO^{i}Pr, and both $LiBF_4$ and LiO^{i}Pr. The

lithium ion-included MOFs exhibited high ionic conductivity in the range 10^{-6}–10^{-4} S cm^{-1} at ambient temperature (30–70 °C). The sample with both $LiBF_4$ and LiO^iPr exhibited the highest ionic conductivity: 3.1×10^{-4} S cm^{-1}. The activation energies were estimated to be in the range 0.14–0.31 eV. These low activation energies suggest that efficient conducing pathways for the lithium ion carrier are formed inside the channels of Mg(dobdc).

Similar example of a lithium ion-conductive MOF with the Type B feature was reported by R. Ameloot et al. They used UiO-66 framework to incorporate lithium salt, Li*O*t*Bu, with a solvent molecule of propylene carbonate.[50] The prepared MOF showed ionic conductivity of 1.8×10^{-5} S cm^{-1} at 20 °C with low activation energy of 0.18 eV.

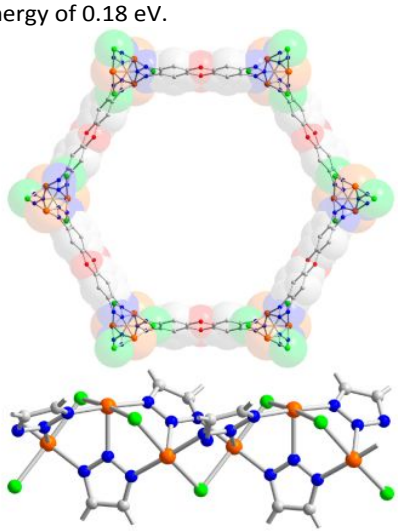

Fig. 20 Representation of the crystal structure of $((CH_3)_2NH_2)[Cu_2Cl_3BTDD]$·guests. Reproduced from ref. 51 with permission from American Chemical Society, copyright 2017.

Park *et al.* reported another example of a Type B compound of a lithium ion-conductive MOF. They synthesized $((CH_3)_2NH_2)[Cu_2Cl_3BTDD]$·Guests ($H_2BTDD$ = bis(1H-1,2,3-triazolo[4,5-*b*],[4′,5′-*i*])dibenzo[1,4]dioxin) as a host framework having open metal sites as Lewis acidic sites (Fig. 20).[51] They introduced lithium ion salts such as LiCl, LiBr and $LiBF_4$ into the MOF with a solvent of propylene carbonate (PC). The anions are expected to be bound by the open metal sites. Thus, this MOF is expected to be suitable for cationic conduction. The lithium ion-included MOFs exhibited high ionic conductivity in the range 10^{-5}–10^{-4} S cm^{-1} (25–70 °C). The MOF that included an additional salt of $LiBF_4$ after inclusion of LiBr had the highest conductivity: 4.8×10^{-4} S cm^{-1}. The activation energies were determined to be in the range 0.16–0.32 eV, suggesting that efficient conducting pathways are formed in this MOF. They also determined the transference number of lithium ions using non-blocking electrodes. This number of lithium ion (t_{Li+}) was estimated to be 0.66, indicating that the lithium ion is the dominant ionic carrier in the conductivity of this MOF.

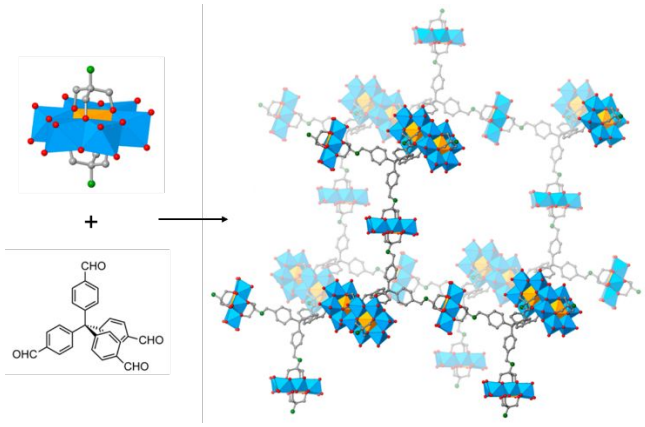

Fig. 21 Representation of the crystal structure and synthetic scheme of MOF-688. Reproduced from ref. 52 with permission from American Chemical Society, copyright 2019.

Xu et al. reported a Type A compound of a lithium ion-conductive MOF, MOF-688, consisting of polyoxometalate $[NBu_4]_3[MnMo_6O_{18}\{(OCH_2)_3CNH_2\}_2]$ and tetrakis(4-formylphenyl)methane.[52] This MOF has anionic framework and showed cation exchange ability. They introduced Li^+ ion into the MOF as a counter cation through an ion exchange reaction with NBu_4^+ ions. They also introduced liquid solvent of propylene carbonate. The prepared sample showed very high ionic conductivity of 3.4×10^{-4} S cm^{-1} at 20 °C. In this MOF, transference number of Li^+ was also determined to be 0.87, which is significantly higher than that of liquid lithium-ion electrolytes. This result clearly indicates that the Type A feature is suitable for increasing the contribution of ionic conduction of the target ions.

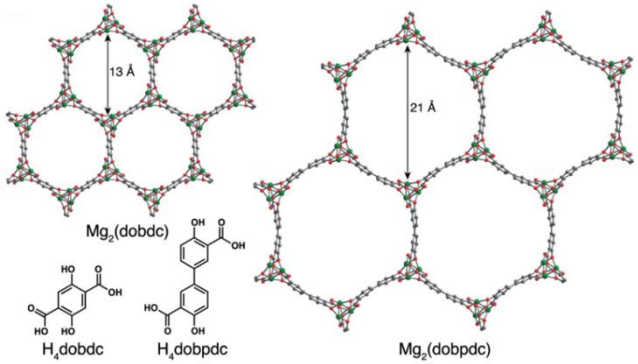

Fig. 22 Schematic illustration of the structure of Mg_2(dobdc) and Mg_2(dobpdc). Reproduced from ref. 53 with permission from Royal Society of Chemistry, copyright 2014.

Magnesium ions are considered to be useful for next-generation secondary batteries because of their abundance (Clarke number 1.93) and potentially high volumetric energy density compared to lithium ion secondary batteries. Aubrey *et al.* reported magnesium ion conduction in the MOFs, Mg_2(dobdc) and Mg_2(dobpdc) ($dobpdc^{4-}$ = 4,4′-dioxidobiphenyl-3,3-dicarboxylate), incorporating magnesium ions with counter ions such as $TFSI^-$ ($TFSI^-$: bis(trifluoromethanesulfonyl)imide) and $OPhCF_3^-$ together with triglyme as a guest molecule (Fig. 22).[53] These MOFs can be also classified as a Type B compound.

Mg_2(dobdc) with these Mg salts and triglyme exhibited ionic conductivity in the range 10^{-9}–10^{-4} S cm^{-1}. Mg_2(dobpdc), having larger pores than Mg_2(dobdc), tended to have higher conductivity, in the range 10^{-7}–10^{-4} S cm^{-1}. The highest conductivity was observed in Mg_2(dobpdc)·0.46Mg(TFSI)$_2$·0.21Mg(OPhCF$_3$)$_2$·4.8triglyme (2.5×10^{-4} S cm^{-1}). The authors mention that the Lewis acidic site in these mother frameworks might bind the anions. The activation energies of these MOFs were in the range 0.11–0.19 eV, suggesting that an efficient conducing pathway for the magnesium ion carrier is also formed in the channels of both Mg(dobdc) and Mg_2(dobpdc).

The [Cu_2Cl_3BTDD]$^-$ framework, mentioned in the lithium ion-conductive MOF, also exhibited ionic conductivity due to sodium and magnesium ions.[51] The ionic conductivity of Na[Cu_2Cl_2(SCN)BTDD]·9(PC) was 1.8×10^{-5} S cm^{-1} with an activation energy of 0.39 eV; these values were similar to those recorded for the lithium ion-included compound, Li[Cu_2Cl_3BTDD]·10(PC). Furthermore, a magnesium ion-included MOF, $Mg_{0.5}$[Cu_2Cl_2BrBTDD]·8(PC), exhibited an ionic conductivity of 8.8×10^{-7} S cm^{-1}, which is slightly lower than that of lithium or sodium ion-included compounds. The activation energy of the magnesium ion-included compound was estimated to be 0.37 eV, which is similar to the other ionic carriers.

Because most of these MOFs that include Li^+, Na^+ and Mg^{2+} cations together include anions such as Cl^-, Br^- and $TFSI^-$ in their pores, it is unclear whether the ionic conductivities mentioned above are derived from the cation conduction or from the anion conduction. Determination of the transference number, using a non-blocking electrode, is required to clarify this issue. In some cases of lithium ion-included MOFs such as Li[Cu_2Cl_3BTDD]·10(PC), the transference number of Li^+ (t_{Li+}) was estimated using a metallic lithium electrode.[51,52] For other ionic carriers such as Mg^{2+}, further investigations appear to be required in order to obtain more information on the conductive properties of the MOFs.

As described above, highly ion-conductive MOFs with the ions other than H^+ or OH^- (i.e., Li^+, Na^+ and Mg^{2+}) was achieved using less volatile liquid solvents such as propylene carbonate (PC). This fact would cause further discussion similar to the case with the grain boundary contribution in proton conduction because the existence of the liquid phase outside the microcrystals of MOFs also has a potential to act as a good ion-conducting pathway for Li^+, Na^+ and Mg^{2+}. This point is more unclear in the case of Li^+, Na^+ or Mg^{2+} ion-conducive MOFs compared to the proton-conductive MOFs at the moment. In addition, the inner structures of salt-included MOFs were hardly determined because of the disordered structures of the included salts, while the inner structures of proton-conductive MOFs have been often completely determined in many cases. Related to this point, in most of the cases of ion-conductive MOFs with Li^+, Na^+ and Mg^{2+}, it is not confirmed whether the salts and solvents were introduced inside the pore of MOFs or not (i.e., mainly located outside of MOFs). This point should be carefully considered to estimate bulk conductivity of MOFs. Some researchers also achieved very high ionic conductivity using ionic liquids with Li^+ or Na^+ salts, which are impregnated with MOFs.[54–57] This kind of approaches seems successful to obtain high ionic conductivity of samples (above 10^{-4} S cm^{-1}) at ambient temperature. However, in these cases, contribution of bulk conductivity of MOFs to whole ionic conductivity of the samples become more unclear because ionic liquids have liquid-phase character, ionic conductivity by itself, and ability to help migration of other solvated ions. Additionally, the impregnated components such as some acids, guest molecules (imidazole), solvents, salts and ionic liquids would be desorbed from the pore of MOFs, depending on operating conditions (e.g., temperature, outer atmosphere, or outer environment). This point should be also carefully considered in the case of MOF-based ionic conductors. Towards the applications of the MOFs for some devices such as fuel cells or secondary battery, there also exist some issues that should be carefully considered. For example, fuel cell operation often needs highly humidified condition, however, some MOFs easily decompose by the water vapour. In addition, fuel crossover in MOFs would also become problem for the actual use. As another example, in the case of secondary battery, electrochemical stability of MOFs should be carefully considered because MOFs sometimes include redox-active components in both central metals and bridging ligands.

Conclusions

The porous structures of MOFs provide highly efficient ion-conducting pathways for ionic carriers. For proton-conductive MOFs, the methodology for introducing acidic species is classified into three types, while the introduction of other ionic carriers is classified into two types. Proton conductivity of MOFs reaches >10^{-2} S cm^{-1}, which is comparable to values achieved with practical organic polymers. The highly proton-conductive MOFs can also provide clear information about the visualized structures of the proton-conducting pathways due to their high crystallinity. The conductivity of hydroxide ion-included MOFs also reached ~10^{-2} S cm^{-1}. However, the relationship between conductive properties and structural features has not been deeply investigated (compared with proton conduction). There are fewer reports on ion-conductive MOFs with other ionic carriers such as Li^+, Na^+ and Mg^{2+} than on proton or hydroxide ion-conductive MOFs. In this regard, better insight into the ionic conduction of these carriers in solids holds increasing interest, particularly for the development of solid-state electrolytes for high-performance secondary batteries. The conductivity of these ions in MOFs reaches about 10^{-4} S cm^{-1}, which is still relatively low compared to the conductivity of protons or hydroxide ions. Although this might be due to differences in the conduction mechanism, further investigation should ultimately result in the achievement of higher ionic conductivity of various ionic carriers, such Li^+, Na^+ or Mg^{2+}.

Conflicts of interest

The authors have no conflicts of interest to declare.

Acknowledgements

This work is partially supported by JSPS KAKENHI Grant Nos. 24850013 and 26810037, ACCEL (JST) program, JPMJAC1501, and Grant-in-Aid for Specially Promoted Research (20H05623).

References

1 Y. Kato, S. Hori, T. Saito, K. Suzuki, M. Hirayama, A. Mitsui, M. Yonemura, H. Iba, R. Kanno, *Nat. Energy*, 2016, **1**, 16030.
2 C. Duan, R. J. Kee, H. Zhu, C. Karakaya, T. Chen, S. Ricote, A. Jarry, E. J. Crumlin, D. Hook, R. Braun, N. P. Sullivan, R. O'Hayre, *Nature*, 2018, **557**, 217–222.
3 J. Janek, W. G. Zeier, *Nat. Energy*, 2016, **1**, 16141.; C. Duan, R. J. Kee, H. Zhu, N. Sullivan, L. Zhu, L. Bian, D. Jennings, R. O'Hayre, *Nat. Energy*, 2019, **4**, 230–240.
4 T. Takahashi, H. Iwahara, *Energy Conv.*, 1971, **11**, 105–111.
5 W. Schmidt, H. D. Lutz, *Ber. Bunsenges. Phys. Chem.*, 1984, **88**, 720–723.
6 B. A. Boukamp, R. A. Huggins, *Phys. Lett. A*, 1976, **4**, 231–233.
7 J. B. Goodenough, *Proc. R. Soc. Lond. A*, 1984, **393**, 215–234.
8 G. M. Brown, D. A. Schwinn, J. B. Bates, W. E. Brundage, *Solid State Ionics*, 1981, **5**, 147–150.
9 G. Eckold, K. Funke, J. Kalus, R. E. Lechner, *J. Phys. Chem. Solids*, 1976, **37**, 1097–1103.
10 D. K. Hohnke, *Solid State Ionics*, 1981, **5**, 531–534.; A. Eichler, *Phys. Rev. B*, 2001, **64**, 174103.
11 H. Furukawa, K. E. Cordova, M. O'Keeffe, O. M. Yaghi, *Science*, 2013, **341**, 1230444.
12 R. B. Getman, Y.-S. Bae, C. E. Wilmer, R. Q. Snurr, *Chem. Rev.*, 2012, **112**, 703–723.
13 Q. Qian, P. A. Asinger, M. J. Lee, G. Han, K. M. Rodriguez, S. Lin, F. M. Benedetti, A. X. Wu, W. S. Chi, Z. P. Smith, *Chem. Rev.*, 2020, **120**, 8161–8266.
14 J. Lee, O. K. Farha, J. Roberts, K. A. Scheidt, S. T. Nguyen, J. T. Hupp, *Chem. Soc. Rev.*, 2009, **38**, 1450–1459.
15 J. D. Rocca, D. Liu, W. Lin, *Acc. Chem. Res.*, 2011, **44**, 957–968.
16 N. Agmon, *Chem. Phys. Lett.*, 1995, 244, 456–462.
17 P. W. Atkins, Physical Chemistry 6th edition, 806.
18 K. D. Kreuer, A. Rabenau, W. Weppner, *Angew. Chem., Int. Ed.*, 1982, 21, 208–209.
19 H.-G. Haubold, T. V. H. Jungbluth, P. Hiller, *Electrochim. Acta*, 2001, **46**, 1559–1563.
20 B. C. Wood, N. Marzari, *Phys. Rev. B*, 2007, **76**, 134301–134313.
21 K. D. Kreuer, *Annu. Rev. Mater. Res.*, 2003, **33**, 333–359.
22 S. Kanda, K. Yamashita, K. Ohkawa, *Bull. Chem. Soc. Jpn.*, 1979, **52**, 3296–3301.
23 M. Fujishima, S. Kanda, T. Mitani, H. Kitagawa, *Synth. Met.*, 2001, **119**, 485–486.; Y. Nagao, R. Ikeda, S. Kanda, Y. Kubozono, H. Kitagawa, *Mol. Cryst. Liq. Cryst.*, 2002, **379**, 89–94.; H. Kitagawa, Y. Nagao, M. Fujishima, R. Ikeda, S. Kanda, *Inorg. Chem. Commun.*, 2003, **6**, 346–348.; Y. Nagao, M. Fujishima, R. Ikeda, S. Kanda, H. Kitagawa, *Synth. Met.*, 2003, **133**, 431–432.; Y. Nagao, R. Ikeda, K. Iijima, T. Kubo, K. Nakasuji, H. Kitagawa, *Synth. Met.*, 2003, **135**, 283–284.; Y. Nagao, T. Kubo, K. Nakasuji, R. Ikeda, T. Kojima, H. Kitagawa, *Synth. Met.*, 2005, **154**, 89–92.
24 M. Sadakiyo, T. Yamada, H. Kitagawa, *J. Am. Chem. Soc.*, 2009, **131**, 9906–9907.
25 S. Bureekaew, S. Horike, M. Higuchi, M. Mizuno, T. Kawamura, D. Tanaka, N. Yanai, S. Kitagawa, *Nature Mater.*, 2009, **8**, 831–836.
26 J. A. Hurd, R. Vaidhyanathan, V. Thangadurai, C. I. Ratcliffe, I. L. Moudrakovski, G. K. H. Shimizu, *Nat. Chem.*, 2009, **1**, 705–710.
27 P. Ramaswamy, N. E. Wong, G. K. H. Shimizu, *Chem. Soc. Rev.*, 2014, **43**, 5913–5932.
28 M. Sadakiyo, T. Yamada, K. Honda, H. Matsui, H. Kitagawa, *J. Am. Chem. Soc.*, 2014, **136**, 7701–7707.
29 M. Sadakiyo, T. Yamada, H. Kitagawa, *J. Am. Chem. Soc.*, 2014, **136**, 13166–13169.
30 S. Miyatsu, M. Kofu, A. Nagoe, T. Yamada, M. Sadakiyo, T. Yamada, H. Kitagawa, M. Tyagi, V. G. Sakai, O. Yamamuro, *Phys Chem. Chem. Phys.*, 2014, **16**, 17295–17304.
31 H. Tamaki, Z. J. Zhong, N. Matsumoto, S. Kida, M. Koikawa, N. Achiwa, Y. Hashimoto, H. Ōkawa, *J. Am. Chem. Soc.*, 1992, **114**, 6974–6979.
32 H. Ōkawa, A. Shigematsu, M. Sadakiyo, T. Miyagawa, K. Yoneda, M. Ohba, H. Kitagawa, *J. Am. Chem. Soc.*, 2009, **131**, 13516–13522.
33 M. Sadakiyo, H. Ōkawa, A. Shigematsu, M. Ohba, T. Yamada, H. Kitagawa, *J. Am. Chem. Soc.*, 2012, **134**, 5472–5475.
34 H. Ōkawa, M. Sadakiyo, T. Yamada, M. Maesato, M. Ohba, H. Kitagawa, *J. Am. Chem. Soc.*, 2013, **135**, 2256–2262.
35 A. Shigematsu, T. Yamada, H. Kitagawa, *J. Am. Chem. Soc.*, 2011, **133**, 2034–2036.
36 W. J. Phang, H. Jo, W. R. Lee, J. H. Song, K. Yoo, B. Kim, C. S. Hong, *Angew. Chem. Int. Ed.*, 2015, **54**, 5142–5146.
37 J. M. Taylor, K. W. Dawson, G. K. H. Shimizu, *J. Am. Chem. Soc.*, 2013, **135**, 1193–1196.
38 N. E. Wong, P. Ramaswamy, A. S. Lee, B. S. Gelfand, K. J. Bladek, J. M. Taylor, D. M. Spasyuk, G. K. H. Shimizu, *J. Am. Chem. Soc.*, 2017, **139**, 14676–14683.
39 S. Tominaka, A. K. Cheetham, *RSC Adv.*, 2014, **4**, 54382–54387.
40 G. Xu, K. Otsubo, T. Yamada, S. Sakaida, H. Kitagawa, *J. Am. Chem. Soc.*, 2013, **135**, 7438–7441.
41 J. M. Taylor, S. Dekura, R. Ikeda, H. Kitagawa, *Chem. Mater.*, 2015, **27**, 2286–2289.
42 K. Otake, K. Otsubo, T. Komatsu, S. Dekura, J. M. Taylor, R. Ikeda, K. Sugimoto, A. Fujiwara, C.-P. Chou, A. W. Sakti, Y. Nishimura, H. Nakai, H. Kitagawa, *Nat. Commun.*, 2020, **11**, 843.
43 D. Umeyama, S. Horike, M. Inukai, T. Itakura, S. Kitagawa, *J. Am. Chem. Soc.*, 2012, **134**, 12780–12785.
44 M. E. Tuckerman, D. Marx, M. Parrinello, *Nature*, 2002, **417**, 925–929.
45 M. Sadakiyo, H. Kasai, K. Kato, M. Takata, M. Yamauchi, *J. Am. Chem. Soc.*, 2014, **136**, 1702–1705.
46 K. S. Park, Z. Ni, A. P. Cote, J. Y. Choi, R. Huang, F. J. Uribe-Romo, H. K. Chae, M. O'Keeffe, O. M. Yaghi, *PNAS*, 2006, **103**, 10186–10191.
47 Z. Li, Z. Zhang, Y. Ye, K. Cai, F. Du, H. Zeng, J. Tao, Q. Lin, Y. Zheng, S. Xiang, *J. Mater. Chem. A*, 2017, **5**, 7816–7824.
48 S. S. Nagarkar, B. Anothumakkool, A. V. Desai, M. M. Shirolkar, S. Kurungot, S. K. Ghosh, *Chem. Commun.*, 2016, **52**, 8459–8462.
49 B. M. Wiers, M.-L. Foo, N. P. Balsara, J. R. Long, *J. Am. Chem. Soc.*, 2011, **133**, 14522–14525.
50 R. Ameloot, M. Aubrey, B. M. Wiers, A. P. G.-Figueroa, S. N. Patel, N. P. Balsara, J. R. Long, *Chem. Eur. J.,* **2013**, *19*, 5533–5536.
51 S. S. Park, Y. Tulchinsky, M. Dinca, *J. Am. Chem. Soc.*, 2017, **139**, 13260–13263.
52 W. Xu, X. Pei, C. S. Diercks, H. Lyu, Z. Ji, O. M. Yaghi, *J. Am. Chem. Soc.*, **2019**, *141*, 17522–17526.
53 M. L. Aubrey, R. Ameloot, B. M. Wiers, J. R. Long, *Energy Environ. Sci.*, 2014, **7**, 667–671.
54 K. Fujie, R. Ikeda, K. Otsubo, T. Yamada, H. Kitagawa, *Chem. Mater.*, 2015, **27**, 7355–7361.
55 Z. Wang, R. Tan, H. Wang, L. Yang, J. Hu, H. Chen, F. Pan, *Adv. Mater.,* 2018, **30**, 1704436.
56 V. Nozari, C. Calahoo, J. M. Tuffnell, P. Adelhelm, K.

Wondraczek, S. E. Dutton, T. D. Bennett, L. Wondraczek, *Sci. Rep.*, 2020, **10**, 3532.
57 Q. Xu, F. Yang, X. Zhang, J.-R. Li, J.-F. Chen, S. Zhang, *ChemElectroChem*, 2020, **7**, 183–190.